JACS
JOURNAL OF THE AMERICAN CHEMICAL SOCIETY
Article
pubs.acs.org/JACS

Aqueous Phase Synthesis of Au–Ag Core–Shell Nanocrystals with Tunable Shapes and Their Optical and Catalytic Properties

Yu-Chi Tsao, Sourav Rej, Chun-Ya Chiu, and Michael H. Huang*

Department of Chemistry, National Tsing Hua University, Hsinchu 30013, Taiwan

Supporting Information

ABSTRACT: In this study, rhombic dodecahedral gold nanocrystals were used as cores for the generation of Au–Ag core–shell nanocrystals with cubic, truncated cubic, cuboctahedral, truncated octahedral, and octahedral structures. Gold nanocrystals were added to an aqueous mixture of cetyltrimethylammonium chloride (CTAC) surfactant, $AgNO_3$, ascorbic acid, and NaOH to form the core–shell nanocrystals. The nanocrystals are highly uniform in size and shape, and can readily self-assemble into ordered packing structures on substrates. Results from observation of solution color changes and variation in the reaction temperature suggest octahedra are produced at a higher growth rate, while slower growth favors cube formation. The major localized surface plasmon resonance (LSPR) band positions for these nanocrystals are red-shifted compared to those for pristine silver particles with similar dimensions due to the LSPR effect from the gold cores. By increasing the concentrations of reagents, Au–Ag core–shell cubes and octahedra with tunable sizes were obtained. Au–Ag cubes with body diagonals of 130, 144, and 161 nm and octahedra with body diagonals of 113, 126, and 143 nm have been prepared, allowing the investigation of size effect on their optical properties. Au–Ag octahedra with thinner Ag shells (12–16.5 nm) exhibit a blue-shifted major LSPR band relative to the LSPR band at 538 nm for the gold cores. For Au–Ag octahedra and cubes with thicker shells (22.5–37 nm), the major LSPR band is progressively red-shifted from that of the gold cores with increasing shell thickness and particle size. The Au–Ag octahedra show higher catalytic activity than cubes toward reduction of 2-amino-5-nitrophenol by $NaBH_4$ at 30 °C, but both particle shapes display significantly enhanced catalytic efficiency at 40 °C.

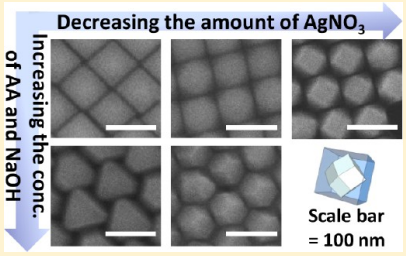

INTRODUCTION

Gold and silver nanocrystals are an important class of nanomaterials due to their strong size- and shape-dependent LSPR properties and ability to bind a wide variety of organic and biological molecules for potential applications in chemical sensing, photothermal therapy, and as sensitive substrates for surface-enhanced Raman scattering (SERS) of adsorbed molecules.[1−5] Catalytic activity of silver nanostructures exposing different crystal faces for the oxidation of styrene has also been examined.[6] For the synthesis of silver nanocrystals with tunable shapes from cubic to octahedral structures, a polyol process has generally been employed. Silver precursor added to a solution of ethylene glycol or 1,5-pentanediol in the presence of capping polymer such as poly(vinyl pyrrolidone), or PVP, is normally heated to 150–180 °C.[7−9] The initially produced silver nanocubes are transformed into truncated cubes, cuboctahedra, and octahedra by controlling the reaction time.[7,8] The polyol synthetic approach suffers from elaborate PVP removal steps, high reaction temperature, and large sizes of the synthesized octahedra (250–300 nm). Development of aqueous phase synthesis of silver nanocrystals using simple surfactant should be quite important. However, silver polyhedra formed in aqueous solutions are mostly cubes as far as a series of particle shape transition from cubic to octahedral morphologies is concerned.[10] It remains challenging to synthesize silver nanocrystals in aqueous solution with systematic shape tuning from cubic to octahedral morphologies. An alternative strategy to achieving this goal is by making Au–Ag core–shell heterostructures. While various Au–Ag core–shell nanostructures can be synthesized using a polyol process in the presence of PVP,[11−13] formation of Au–Ag core–shell nanocrystals in aqueous solution has also been achieved.[14−22] However, mainly nanocubes were produced with the use of polyhedral gold cores in aqueous solution. Other shapes such as Au–Ag core–shell octahedra and tetrahedra can be obtained by a light-induced synthetic approach.[21] Interestingly, use of decahedral gold nanocrystals as cores can yield Au–Ag nanorods, while gold nanoplate cores give elongated Au–Ag structures.[23−26] Clearly, the growth of Au–Ag core–shell nanocrystals with systematic shape evolution from cubic to octahedral structures in aqueous solution using polyhedral gold cores has not been achieved yet. Furthermore, it is highly desirable that the synthesized Au–Ag nanocrystals show excellent size and shape control for their large-scale assembly and comparison of their optical and catalytic properties.

In this study, we have successfully synthesized Au–Ag core–shell nanocubes, truncated cubes, cuboctahedra, truncated octahedra, and octahedra in aqueous solution using rhombic dodecahedral gold nanocrystals as cores. The particles are highly uniform in size and shape that they spontaneously self-

Received: October 18, 2013
Published: December 17, 2013

   dx.doi.org/10.1021/ja410663g | J. Am. Chem. Soc. 2014, 136, 396–404

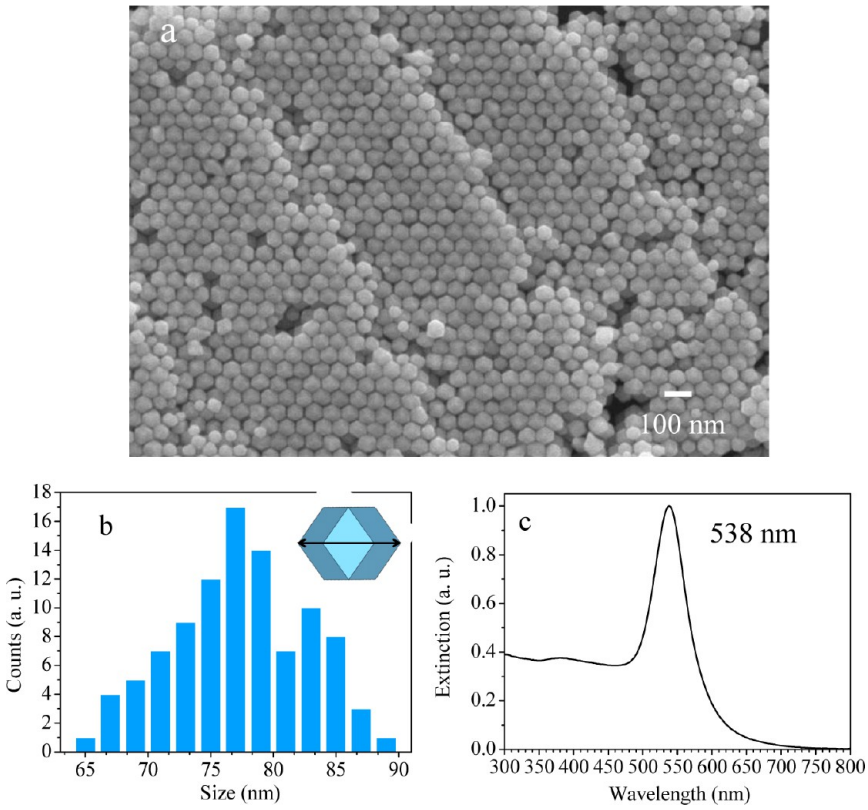

Figure 1. (a) SEM image of the synthesized rhombic dodecahedral gold nanocrystals. (b) Size distribution histogram and a drawing of the particle. The arrow indicates the particle size. (c) UV–vis absorption spectrum of the rhombic dodecahedral gold nanocrystals.

assemble on substrates. The relative growth rates in the formation of nanocubes and octahedra have been evaluated by visual observation of solution color changes and adjustment of reaction temperature. Sizes of the nanocubes and octahedra can also be tuned over a range. Optical property characterization of the particles has been performed. Interestingly, both blue-shifts and red-shifts of the core–shell plasmonic band relative to those of the Au cores have been recorded. Facet-dependent catalytic activity of the Au–Ag nanocubes and octahedra was also examined through borohydride reduction of 2-amino-5-nitrophenol.

EXPERIMENTAL SECTION

Synthesis of Cubic, Truncated Cubic, and Cuboctahedral Au–Ag Core–Shell Nanocrystals. The rhombic dodecahedral gold nanocrystals with an average size of 53 nm were prepared following our reported method.[27] In a typical synthesis of Au–Ag core–shell nanocubes, 0.064 g of CTAC surfactant, 9.46 mL of deionized water, and 40 μL of the Au rhombic dodecahedra solution were introduced. The vial was kept in a water bath set at 30 °C. Then 50 μL of 0.01 M $AgNO_3$ solution was added into the sample vial. For the growth of truncated cubic and cuboctahedral Au–Ag core–shell nanocrystals, 40 and 30 μL, respectively, of 0.01 M $AgNO_3$ solution were introduced into the reaction mixture. Finally, 150 μL of 0.0175 M ascorbic acid solution and 300 μL of 0.0175 M NaOH solution were added. Immediately after the addition of NaOH, the solution turned from pink to yellow within 1 min. After 50 min, the solution was centrifuged at 3500 rpm for 10 min.

Synthesis of Truncated Octahedral and Octahedral Au–Ag Core–Shell Nanocrystals. Truncated octahedral and octahedral Au–Ag core–shell nanocrystals were synthesized using the same amounts of CTAC and Au rhombic dodecahedra solution. However, 150 μL of 0.05 M ascorbic acid solution and 300 μL of 0.05 M NaOH solution were added. Here 35 and 50 μL of 0.01 M $AgNO_3$ solution were used for the growth of truncated octahedra and octahedra, respectively. After further reaction for 50 min, the solution was centrifuged at 3500 rpm for 10 min. An illustration of the synthetic procedure used is given in Scheme S1.

Synthesis of Cubic and Octahedral Au–Ag Core–Shell Nanocrystals with Tunable Size. The above procedures described yield Au–Ag core–shell nanocubes and nanooctahedra with edge lengths of 75 and 81 nm, respectively. To make larger nanocubes and octahedra, the same volume of Au rhombic dodecahedra solution was used (40 μL), but the amounts of other reagents used were increased. For the synthesis of Au–Ag nanocubes with edge lengths of 83 and 93 nm, the amount of CTAC and the concentrations of $AgNO_3$ solution, ascorbic acid solution and NaOH solution added were 1.5 and 2 times those used to make 75 nm nanocubes, respectively. Similarly, to obtain octahedra with edge lengths of 90 and 102 nm, the amount of CTAC and the concentrations of $AgNO_3$ solution, ascorbic acid solution and NaOH solution added were 1.5 and 2 times those used to make 81 nm octahedra, respectively. A scheme summarizing the experimental procedure is available in Scheme S2.

Catalytic Reduction of 2-Amino-5-nitrophenol. For a typical catalysis reaction, 1 mL of 1.0×10^{-3} M 2-amino-5-nitrophenol solution was added to 8 mL of deionized water and stirred thoroughly. After that, different volumes of the Au–Ag nanocrystal solutions were added to the reaction mixture (i.e., 300 μL for nanocubes and 148 μL for octahedra), keeping the total surface area of the core–shell particles approximately the same at around 10.78 cm^2 (see Table S1). The reaction mixture was maintained at 30 °C using a water bath. Finally, 2.4 mL of 0.1 M ice-cold $NaBH_4$ solution was added and the solution was mixed well to start the reaction. Next, 800 μL of the reaction mixture was transferred to a narrow-slit cuvette for spectral measurements without dilution. The solution was discarded after taking a spectrum and fresh solution from the same reaction mixture was used for the next measurement. UV–vis absorption spectra were recorded at different time periods depending on the reaction rate. After the completion of the reduction reaction, the yellowish 2-amino-

dx.doi.org/10.1021/ja410663g | J. Am. Chem. Soc. 2014, 136, 396–404

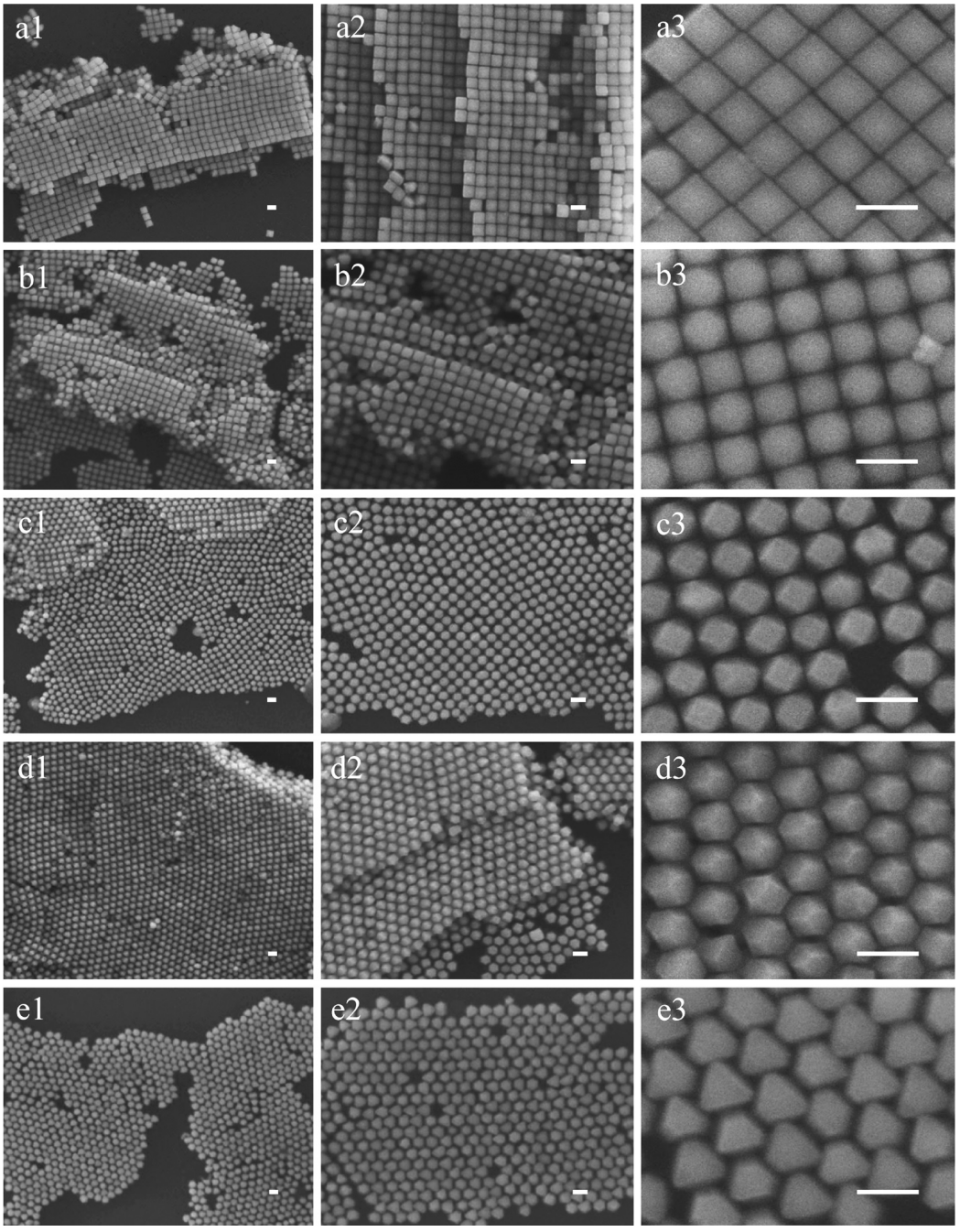

Figure 2. SEM images of Au−Ag core−shell (a1−a3) nanocubes, (b1−b3) truncated cubes, (c1−c3) cuboctahedra, (d1−d3) truncated octahedra, and (e1−3) octahedra viewed at different magnifications. All scale bars are equal to 100 nm.

5-nitrophenol solution turned colorless due to the formation of 2,5-diaminophenol product.

Instrumentation. Scanning electron microscopy (SEM) images of the samples were obtained using a JEOL JSM-7000F electron microscope. Transmission electron microscope (TEM) characterization was performed on a JEOL JEM-2100 microscope with an operating voltage of 200 kV. Elemental mapping images were acquired by energy-dispersive X-ray spectroscopy (EDS) using the same JEOL JEM-2100 electron microscope equipped with a STEM unit and an Inca Energy 250 detector from Oxford Instruments. Powder X-ray diffraction (XRD) patterns were recorded on a Shimadzu XRD-6000 diffractometer with Cu Kα radiation. UV−vis absorption spectra were taken using a JASCO V-670 spectrophotometer.

RESULTS AND DISCUSSION

Our goal in the preparation of Au−Ag core−shell nanocrystals is to achieve their systematic shape evolution from cubic to octahedral structures for possible assembly and facet-dependent property investigation.[28,29] The relative growth rates needed to form different particle morphologies can also be studied. Here rhombic dodecahedral gold nanocrystals were employed for the preparation of Au−Ag core−shell nanocrystals. The particles were synthesized following a seed-mediated growth method in the presence of a tiny amount of NaBr.[27] Figure 1 illustrates the SEM image of the synthesized rhombic dodecahedral Au nanocrystals with an average edge length of 33 or 77 nm by measuring the opposite corner-to-corner distance. Because of

dx.doi.org/10.1021/ja410663g | J. Am. Chem. Soc. 2014, 136, 396−404

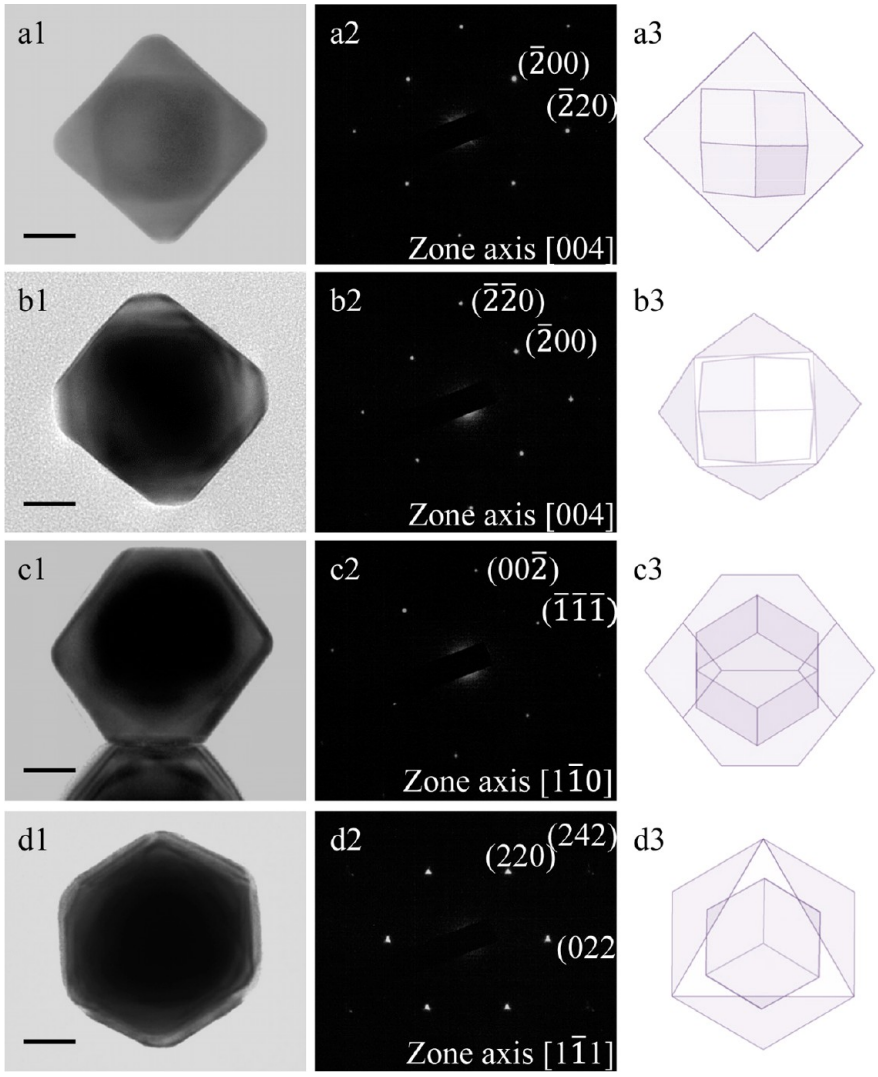

Figure 3. TEM images, corresponding SAED patterns, and representative drawings of single Au−Ag core−shell (a1−a3) cube, (b1−b3) cuboctahedron viewed along the [100] direction, (c1−c3) truncated octahedron viewed along the [110] direction, and (d1−d3) octahedron viewed along the [111] direction. All scale bars are equal to 20 nm. The triangular diffraction spots seen in panel d2 may be due to double diffraction because of the polyhedral core and shell nature. Split diffraction spot effect is also visible in panel b2.

their uniform size and shape, these particles readily self-assemble into a multilayered packing structure with their ⟨111⟩ axis perpendicular to the substrate plane. They have been demonstrated to pack into supercrystals with micrometer dimensions.[30] The rhombic dodecahedra give a sharp LSPR band at 538 nm. The same rhombic dodecahedral gold nanoparticles can also be obtained by introducing KI instead of NaBr.[31]

To make the Au−Ag core−shell nanocrystals, an aqueous solution of CTAC surfactant, rhombic dodecahedral gold nanocrystals, $AgNO_3$, ascorbic acid, and NaOH was prepared and reacted at 30 °C for 50 min to obtain the products. When the volume of 0.01 M $AgNO_3$ solution introduced was reduced from 50 to 40 and 30 μL, Au−Ag nanocubes were transformed into truncated cubes and cuboctahedra. Raising the concentrations of ascorbic acid and NaOH from those employed for the synthesis of nanocubes, Au−Ag octahedra and truncated octahedra were produced with the use of 50 and 35 μL of 0.01 M $AgNO_3$ solution, respectively. Lower ascorbic acid and NaOH concentrations favor the formation of Au−Ag cubes, while higher ascorbic acid and NaOH concentrations facilitate the growth of octahedra. However, it is difficult to simply tune the concentrations of ascorbic acid and NaOH to achieve a single particle shape; a mixture of cuboctahedra and truncated octahedra can form. We found an easier way to obtain the intermediate particle morphologies is to fix the reaction conditions for making Au−Ag cubes and octahedra, and adjust the volume of $AgNO_3$ slightly to yield truncated cubes, cuboctahedra, and truncated octahedra. Figure 2 presents SEM images of the synthesized Au−Ag core−shell cubes, truncated cubes, cuboctahedra, truncated octahedra, and octahedra taken at different magnifications. Highly uniform Au−Ag nanocrystals have been generated in entire five samples, such that they all spontaneously self-assemble into ordered packing arrangements. The cubes, truncated cubes, and cuboctahedra form roughly face-to-face alignment. Alternatively, their alignment can shift within the same layer and between upper and lower layer as have been observed before for Au and PbS nanocubes.[30,32] The octahedra and truncated octahedra can form monolayer with their {111} faces contacting the substrate plane and multilayer packing structures oriented to show their {110} edges. The average particle sizes in terms of body

dx.doi.org/10.1021/ja410663g | J. Am. Chem. Soc. 2014, 136, 396−404

diagonals for the Au−Ag core−shell cubes, truncated cubes, cuboctahedra, truncated octahedra, and octahedra are 130, 103, 100, 89, and 113 nm (or edge lengths of 75, 73, 71, 80, and 81 nm) with standard deviations of 3.5% or less, respectively (see Figures S1 and S2 and Table S2, Supporting Information). Silver polyhedra with these dimensions have not been demonstrated to show such large-scale assembly, proving the success of this synthetic strategy to yield silver nanocrystals with excellent shape control and tunability.

Further structural analysis of these nanocrystals was performed. XRD patterns of the Au−Ag core−shell cubes and truncated cubes showed only the (200) reflection peak (see Figure S3). Au and Ag have nearly identical lattice constants, so the XRD patterns only give one set of reflection peaks. The cuboctahedra exhibited a strong (200) peak and a weak (111) peak. The relative intensities of the (200) and (111) peaks are reversed for the truncated octahedra. For the octahedra, only the (111) peak was observed. These relative peak intensity changes were recorded as a result of preferential deposition of the nanocrystals on their {100} or {111} faces. Figure 3 presents TEM images, the corresponding selected-area electron diffraction (SAED) patterns, and the drawings of single Au−Ag cube, cuboctahedron, truncated octahedron, and octahedron. The gold cores can be seen. These SAED patterns match to that of face-centered-cubic silver. The single-crystalline nature of the silver shell is evident. High-angle annular dark-field scanning TEM (HAADF-STEM) images of the Au−Ag core−shell cubes give better contrast of the core and shell components (see Figure S4). In addition, EDS line scans confirm the composition of the core and shell as Au and Ag.

UV−vis absorption spectra of these Au−Ag core−shell nanocrystals were taken (Figure 4). Since body diagonals are more appropriate and useful than edge lengths to reflect the actual nanocrystal sizes for particles with different morphologies, these numbers are given in Figure 4. The characteristic multiple absorption band feature of silver due to the dipole and quadruple plasmon resonance has been recorded. The nanocubes show four LSPR bands at 346, 403, 481, and 555 nm. Particles with other shapes display only three bands with the major band centered at 521, 524, 526, and 529 nm for truncated octahedra, cuboctahedra, truncated cubes, and octahedra, respectively. The complete peak positions for these particles are available in Table S3. The emergence of the shoulder band at 480 nm for the nanocubes presumably is due to their larger sizes than particles of other shapes. Ag nanocubes with the same edge length of 75 nm have been reported to show LSPR bands at 345, 395, 450, and 515 nm, while Ag octahedra with an edge length of 75 nm display a major LSPR band at 500 nm.[33] Clearly the major LSPR band of the Au−Ag core−shell nanocrystals is red-shifted compared to pristine Ag particles of the same size and shape. The contribution of the gold cores to the major LSPR band position of silver nanocrystals is obvious. The spectral red-shift toward the LSPR band position of the Au core is reasonable because its LSPR property remains despite the presence of a metal shell, but the band position is tuned by the shell composition and thickness.[15,16]

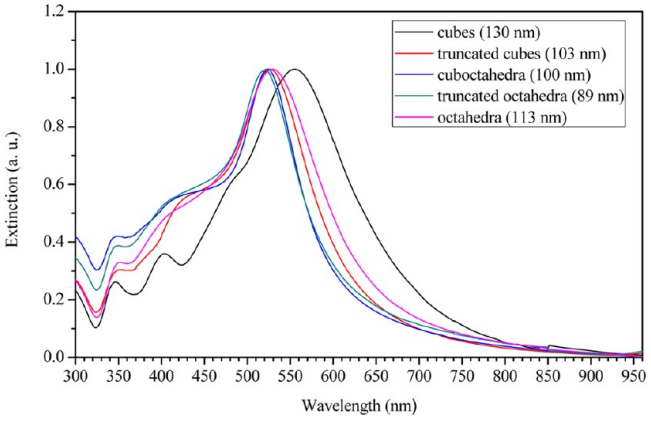

Figure 4. UV−vis-NIR absorption spectra of various synthesized Au−Ag core−shell nanocrystals. Body diagonals are used for the particle sizes.

We have shown previously through nanocrystal synthesis with systematic shape evolution that the formation of different particle shapes is related to their different growth rates.[28] The extent of particle growth can be followed by simply monitoring the solution color changes. Figure S5 presents photographs of the nanocrystal solutions at different time points in the synthesis of Au−Ag core−shell cubes and octahedra. As silver shells are formed, the purplish pink gold nanocrystal solution gradually turns more brightly yellowish. After only 15 s, the solution color remained the same in the formation of octahedra, while it took 39 s for the solution color to become unchanged in the synthesis of cubes. This visual observation suggests that octahedra are formed at a faster growth rate than that for cubes. Mirkin et al. have also found that the formation of different silver particle shapes is related to their different reaction rates.[34,35] The Au−Ag octahedra were produced by introducing higher concentrations of ascorbic acid and NaOH solution than those used for the growth of cubes, implying that a higher reduction or growth rate favors the formation of octahedra, while a slower reduction rate facilitates the generation of cubes. To test this relationship, a reaction condition for the preparation of Au−Ag octahedra was used, but the reaction temperature was decreased from 30 to 20 and 7 °C to reduce the particle growth rate. Remarkably, Au−Ag core−shell cuboctahedra and cubes were respectively synthesized at 20 and 7 °C (see Figure 5). The nanocrystals are also highly uniform in size and shape that they readily self-assemble. The results support the general observation that polyhedral particles with different morphologies are formed at different growth rates, and that a slower rate favors the production of Au−Ag cubes. Thus, nanocrystals with different shapes can be obtained by either varying the ascorbic acid and NaOH concentrations or changing the reaction temperature to tune the particle growth rate. The role of NaOH in enhancing the reducing power of ascorbic acid is explained. Because of the relatively high concentration of CTAC added, $AgNO_3$ should first react with chloride ions to form AgCl. Although ascorbic acid can reduce AgCl to Ag, the reaction rate is too slow. Addition of NaOH can accelerate the reduction reaction and enables better control of the resulting particle shapes. The following equation is the redox reaction taking place between ascorbic acid and Ag^+ ions.

$$\text{ascorbic acid} + 2Ag^+ + H_2O \rightleftharpoons \text{dehydroascorbic acid} + 2H^+ + 2Ag$$

Adding NaOH to the reaction mixture for the growth of silver shells decreases $[H^+]$ and shift the equilibrium to the right, which increases the reducing power of ascorbic acid. Hence,

dx.doi.org/10.1021/ja410663g | J. Am. Chem. Soc. 2014, 136, 396−404

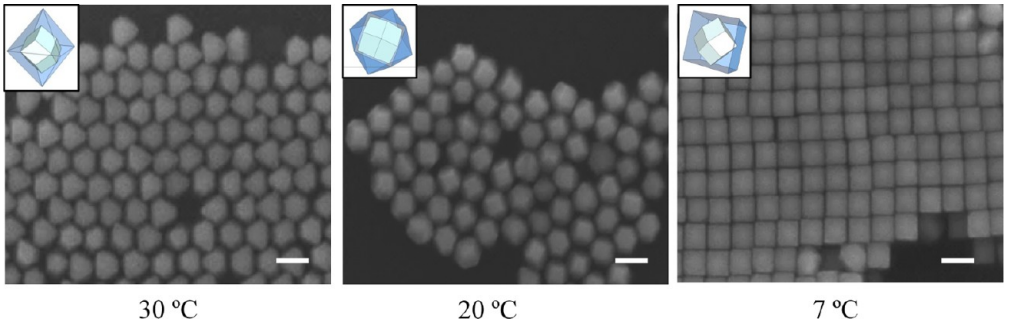

Figure 5. SEM images showing the product shape changes by synthesizing Au−Ag core−shell nanocrystals at different temperatures. The scale bars are equal to 100 nm.

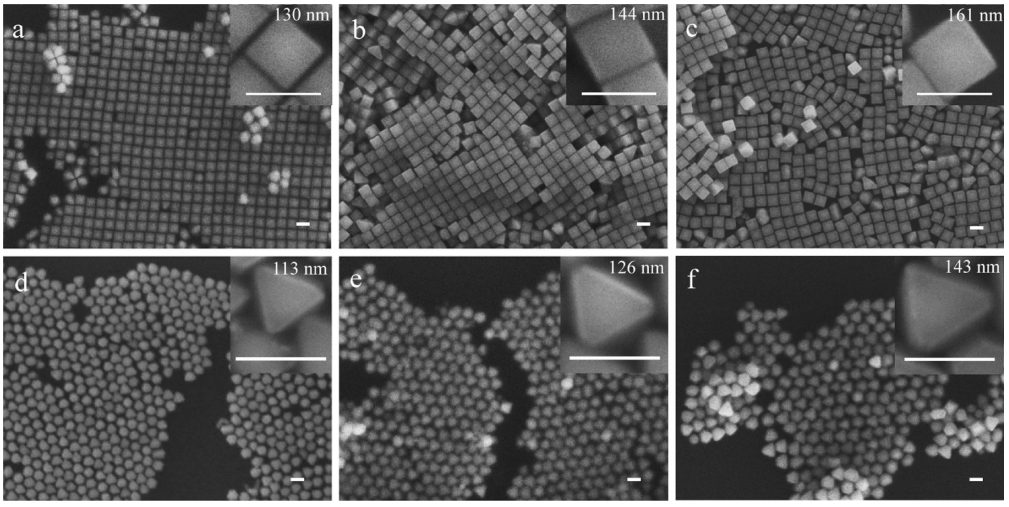

Figure 6. SEM images of the Au−Ag core−shell nanocubes synthesized with body diagonals varying from (a) 130 to (b) 144 and (c) 161 nm and octahedra with body diagonals of (d) 113, (e) 126, and (f) 143 nm. Scale bars are all equal to 100 nm.

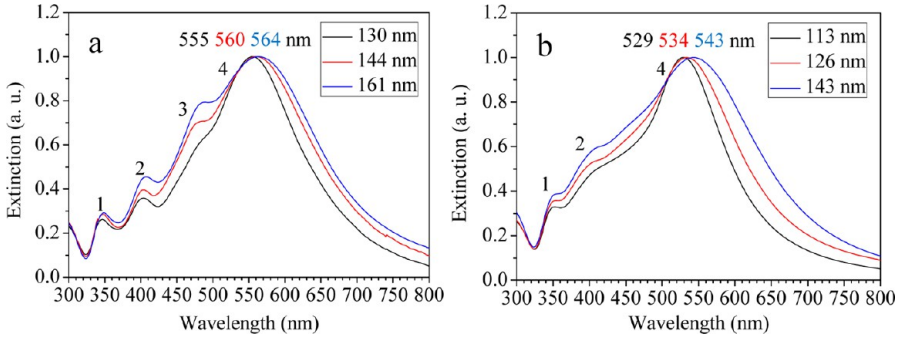

Figure 7. UV−vis absorption spectra of Au−Ag core−shell (a) nanocubes and (b) octahedra with different sizes. Body diagonals are used for particle size.

introduction of different concentrations of NaOH can adjust the redox reaction rate to control the shapes of Au−Ag core−shell nanocrystals.

It is also interesting to make Au−Ag core−shell nanocrystals over a size range by increasing the shell thickness, and see how their LSPR peaks are tuned. When the amount of CTAC and concentrations of $AgNO_3$, ascorbic acid, and NaOH solutions were increased 1.5 and 2 times higher than those used to make Au−Ag core−shell cubes with 130 nm body diagonal, while keeping the volume of rhombic dodecahedral gold nanocrystal solution added constant, Au−Ag core−shell cubes with respective average body diagonals of 144 and 161 nm were prepared. Use of the same synthetic conditions yielded Au−Ag core−shell octahedra with average body diagonals of 126 and 143 nm. Figure 6 is the SEM images of synthesized Au−Ag core−shell cubes and octahedra in this study with three different sizes. Again the larger cubes and octahedra maintain excellent size and shape uniformity that they spontaneously self-assembly into ordered arrays, particularly for octahedra. This high degree of particle size and shape control is extremely important for the accurate examination of size effect on their spectral shifts.

Figure 7 gives UV−vis spectra of the Au−Ag core−shell cubes and octahedra shown in Figure 6. Again body diagonals are provided as this dimension reflects the true particle size better than edge length. The exact peak positions and particle

dx.doi.org/10.1021/ja410663g | J. Am. Chem. Soc. 2014, 136, 396−404

Table 1. Major LSPR Peak Positions and Shifts of Au−Ag Core−Shell Octahedra and Cubes with Different Sizes Relative to the LSPR Peak of the Gold Cores at 538 nm

Oh volume (nm^3)	2.5×10^5	3.4×10^5	5.0×10^5	Cube volume (nm^3)	4.2×10^5	5.7×10^5	8.0×10^5
body diagonal (nm)	113	126	143	body diagonal (nm)	130	144	161
shell thickness (nm)	12	16.5	22.5	shell thickness (nm)	24.5	30	37
major LSPR peak (nm)	529	534	543	major LSPR peak (nm)	555	560	564
LSPR peak shift to Au core peak (nm)	−9	−4	+5	LSPR peak shift to Au core peak (nm)	+17	+22	+26

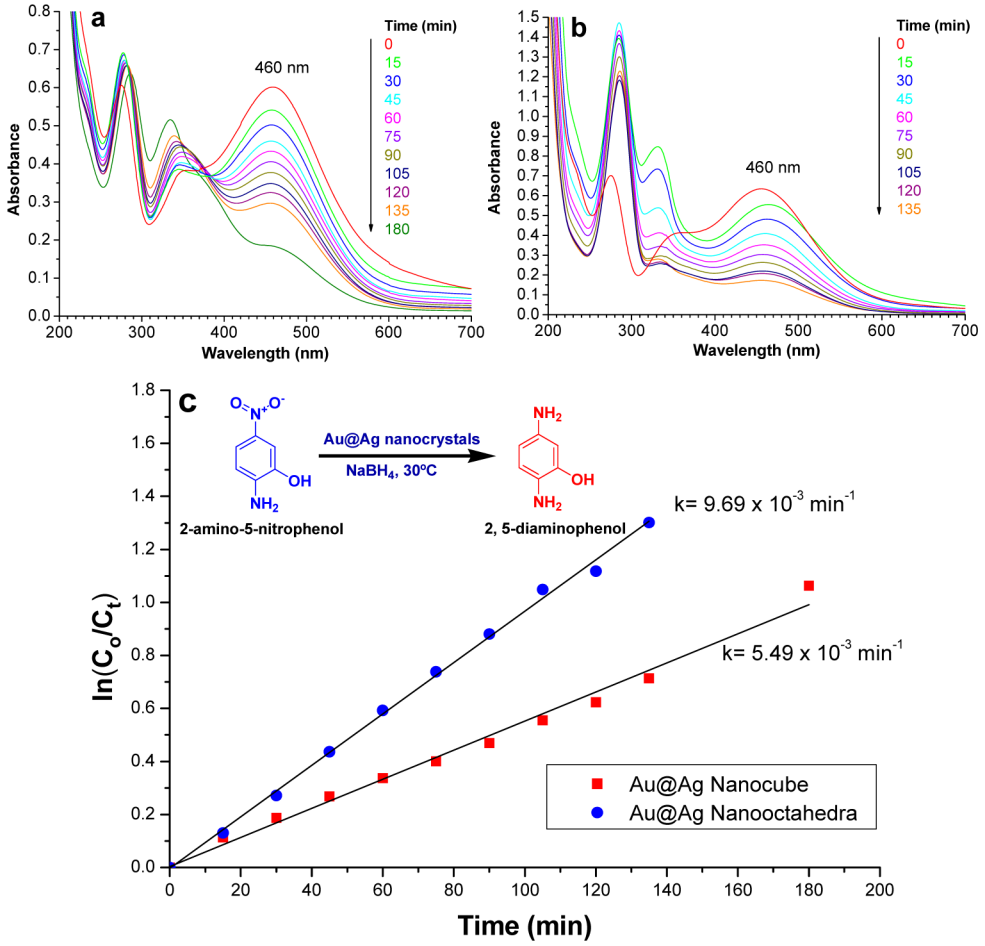

Figure 8. (a and b) Time-dependent UV−vis absorption spectra for the borohydride reduction of 2-amino-5-nitrophenol at 30 °C using Au−Ag core−shell (a) cubes and (b) octahedra. (c) $\ln[C_0/C_t]$ versus time plot using Au−Ag core−shell nanocubes and octahedra as catalysts for the reduction of 2-amino-5-nitrophenol carried out at 30 °C.

sizes in terms of edge length, body diagonal, and single particle volume are available in Table S4. At larger sizes, the cubes show four clearly identifiable peaks, while the shoulder band for the octahedra becomes more pronounced, further indicating the appearance of the shoulder band (or peak 3 for the cubes) in particles with larger dimensions. The spectral shifts of the major LSPR band relative to that of the gold nanocrystal cores are most interesting and insightful to analyze for the size effects. For the Au−Ag core−shell cubes, the major LSPR band red-shifts from 555 to 560 and 564 nm with increasing particle size. Similarly, the major LSPR band red-shifts from 529 to 534 and 543 nm as octahedra become larger. Progressive spectral red-shift with increasing particle size is normal and expected.[9] However, a more careful analysis reveals how the shell thickness can tune the major LSPR band position. Table 1 lists the directions and magnitudes of spectral shifts of the major LSPR band for these Au−Ag core−shell octahedra and cubes relative to the LSPR peak position of the gold cores with consideration of the silver shell thickness (see Figure S6 for the determination of Ag shell thickness). For Au−Ag cubes with Ag shell thicknesses increasing from 24.5 to 30 and 37 nm, the particles show significant red-shifts of 17−26 nm from the absorption band of the Au cores at 538 nm. However, for Au−Ag octahedra with thinner Ag shell thicknesses of 12−22.5 nm, both spectral blue-shift and red-shift were recorded. The 113-nm Au−Ag octahedra with a shell thickness of 12 nm exhibit a blue-shift of 9 nm. Hence, both spectral blue-shift and red-shift can be observed in Au−Ag nanocrystals, and likely in other bimetallic core−shell particles, depending on the shell thickness. Normally the presence of Ag shells shifts the LSPR band of polyhedral Au−Ag core−shell nanocrystals to the blue to reflect the SPR character of silver. However, a large shell thickness results in a significant increase in overall particle size, so absorption bands of the core−shell particles become more red-shifted with growing particle dimensions. It is also interesting to note that the extents of spectral red-shift differ

dx.doi.org/10.1021/ja410663g | J. Am. Chem. Soc. 2014, 136, 396−404

substantially for 143-nm octahedra and 130-nm cubes (5 vs 17 nm), even though the shell thickness difference seems small. This is likely attributed to the fact that the Au core is actually closer to the nanocrystal surface at some points of the core−shell cube than the Au core is in an octahedron (see Figure 3). Hence, the SPR character of the Au core is more pronounced and this leads to a greater peak red shift. Such spectral analysis enhances our understanding of SPR behavior in bimetallic core−shell nanocrystals, and the data are more reliable when the particles have excellent size and shape control.

The Au−Ag core−shell cubes and octahedra exposing exclusively {100} and {111} facets can be used to examine the facet-dependent catalytic activity of silver nanocrystals. Although Ag and Au−Ag core−shell nanoparticles have been tested for catalytic reduction of 4-nitrophenol by $NaBH_4$ in water, facet-dependent catalytic activity investigation was not possible.[36,37] We have previously compared the catalytic activity of gold nanocubes, octahedra, and rhombic dodecahedra toward 4-nitroaniline reduction.[38] Gold rhombic dodecahedra showed the best catalytic activity at all the temperatures examined. Gold nanocubes displayed better catalytic efficiency than octahedra in the temperature range of 25−32 °C, but interestingly octahedra can be somewhat better catalysts than cubes at higher reaction temperatures (36−40 °C). Here, different volumes of the nanocrystal solutions having the same total surface area were used for the comparative catalytic activity experiments (see Supporting Information for the calculations). Figure 8 offers time-dependent UV−vis absorption spectra for the $NaBH_4$ reduction of 2-amino-5-nitrophenol at 30 °C using Au−Ag core−shell cubes and octahedra to mediate electron transfer. The band at 460 nm from 2-amino-5-nitrophenol descreases gradually as the reaction proceeds, while two new bands at 285 and 330 nm from the product 2,5-diaminophenol increase continuously. However, the reaction is still far from completion after 135 min. A plot of $\ln[C_o/C_t]$ versus time for these spectra gives straight lines, indicating the reaction follows first-order kinetics. The Au−Ag octahedra and cubes have respective rate constants of 9.69×10^{-3} min^{-1} and 5.49×10^{-3} min^{-1}, so octahedra are more catalytically active at 30 °C. For the reaction to take place, both BH_4^- and 2-amino-5-nitrophenolate ion should be adsorbed on the particle surface to facilitate electron transfer from BH_4^- to 2-amino-5-nitrophenolate. The surface atom densities of Ag (111) and Ag (100) planes are 13.8 and 12.0 atoms/nm^2, respectively. An octahedron with a higher surface silver atom density can have more reactive sites than a cube for ionic adsorption, so the Au−Ag octahedra are more catalytically active than the cubes. Of course, binding energies of the molecule to different surface planes of a metal can also be determined to evaluate the facet-dependent catalytic activity.[38] Remarkably, the same reaction takes place so rapidly at 40 °C for both the Au−Ag octahedra and cubes that 2-amino-5-nitrophenol is mostly converted after 10 min of reaction (see Figure S7). In fact, the 460 nm band drops more rapidly for cubes than for octahedra after 5 min of reaction, and clearly identifiable product bands are better recorded for the cubes. However, the product band rises more quickly for octahedra. Reversal of relative reactivity is possible for the two particle shapes depending on the reaction temperature. Mostly importantly, both Au−Ag cubes and octahedra become highly efficient catalysts for this reaction at higher temperatures.

CONCLUSION

Rhombic dodecahedral gold nanocrystals were employed as cores for the growth of Au−Ag core−shell nanocrystals with systematic shape evolution from cubic to truncated cubic, cuboctahedral, truncated octahedral, and octahedral structures. The nanocrystals are highly uniform in size and shape that they readily self-assemble on substrates. Silver polyhedra assembly using small particles with edge lengths of 80 nm or less is rare. Thus, synthesis of polyhedral silver nanocrystals, which are quite challenging to prepare in aqueous solution using a simple capping agent such as CTAC surfactant, has been achieved through the core−shell growth strategy. The major LSPR band positions for these nanocrystals are red-shifted compared to pristine silver particles with similar dimensions due to the SPR effect of the gold cores. When the reagent amounts are increased, Au−Ag core−shell cubes and octahedra with tunable sizes can be obtained. With relatively thin silver shells, the major LSPR band of Au−Ag octahedra is blue-shifted relative to that of the gold cores, but becomes progressively red-shifted with increasing shell thickness. Au−Ag octahedra are more catalytically active than cubes toward $NaBH_4$ reduction of 2-amino-5-nitrophenol at 30 °C, but both particle shapes increase their catalytic efficiency significantly at 40 °C. It is envisioned that these particles can be utilized to catalyze many other reactions, assembled to form superlattice structures, and serve as excellent SERS substrates.

ASSOCIATED CONTENT

Supporting Information

Additional experimental procedures, calculations for the catalysis experiments, particle size distribution histograms, XRD patterns, HAADF-TEM image, EDS line scans, and additional SEM images and UV−vis spectra. This material is available free of charge via the Internet at http://pubs.acs.org.

AUTHOR INFORMATION

Corresponding Author

hyhuang@mx.nthu.edu.tw

Notes

The authors declare no competing financial interest.

ACKNOWLEDGMENTS

This work was funded by National Science Council of Taiwan (Grant 101-2113-M-007-018-MY3).

REFERENCES

(1) Mayer, K. M.; Hafner, J. H. *Chem. Rev.* **2011**, *111*, 3828−3857.
(2) McFarland, A. D.; Van Duyne, R. P. *Nano Lett.* **2003**, *3*, 1057−1062.
(3) Hu, K.-W.; Liu, T.-M.; Chung, K.-Y.; Huang, K.-S.; Hsieh, C.-T.; Sun, C.-K.; Yeh, C.-S. *J. Am. Chem. Soc.* **2009**, *131*, 14186−14187.
(4) Mulvihill, M. J.; Ling, X. Y.; Henzie, J.; Yang, P. *J. Am. Chem. Soc.* **2010**, *132*, 268−274.
(5) Wu, H.-L.; Tsai, H.-R.; Hung, Y.-T.; Lao, K.-U.; Liao, C.-W.; Chung, P.-J.; Huang, J.-S.; Chen, I-C.; Huang, M. H. *Inorg. Chem.* **2011**, *50*, 8106−8111.
(6) Xu, R.; Wang, D.; Zhang, J.; Li, Y. *Chem. Asian J.* **2006**, *1*, 888−893.
(7) Xia, X.; Zeng, J.; Oetjen, L. K.; Li, Q.; Xia, Y. *J. Am. Chem. Soc.* **2012**, *134*, 1793−1801.
(8) Tao, A.; Sinsermsuksakul, P.; Yang, P. *Angew. Chem., Int. Ed.* **2006**, *45*, 4597−4601.

(9) Zhang, Q.; Li, W.; Moran, C.; Zeng, J.; Chen, J.; Wen, L.-P.; Xia, Y. *J. Am. Chem. Soc.* **2010**, *132*, 11372−11378.
(10) (a) Yu, D.; Yam, V. W.-W. *J. Am. Chem. Soc.* **2004**, *126*, 13200−13201. (b) Yu, D.; Yam, V. W.-W. *J. Phys. Chem. B* **2005**, *109*, 5497−5503.
(11) (a) Tsuji, M.; Miyamae, N.; Lim, S.; Kimura, K.; Zhang, X.; Hikino, S.; Nishio, M. *Cryst. Growth Des.* **2006**, *6*, 1801−1807. (b) Tsuji, M.; Matsuo, R.; Jiang, P.; Miyamae, N.; Ueyama, D.; Nishio, M.; Hikino, S.; Kumagae, H.; Kamarudin, K. S. N.; Tang, X.-L. *Cryst. Growth Des.* **2008**, *8*, 2528−2536.
(12) Park, G.; Seo, D.; Jung, J.; Ryu, S.; Song, H. *J. Phys. Chem. C* **2011**, *115*, 9417−9423.
(13) Seo, D.; Yoo, C. I.; Jung, J.; Song, H. *J. Am. Chem. Soc.* **2008**, *130*, 2940−2941.
(14) Fan, F.-R.; Liu, D.-Y.; Wu, Y.-F.; Duan, S.; Xie, Z.-X.; Jiang, Z.-Y.; Tian, Z.-Q. *J. Am. Chem. Soc.* **2008**, *130*, 6949−6951.
(15) Gong, J.; Zhou, F.; Li, Z.; Tang, Z. *Langmuir* **2012**, *28*, 8959−8964.
(16) Ma, Y.; Li, W.; Cho, E. C.; Li, Z.; Yu, T.; Zeng, J.; Xie, Z.; Xia, Y. *ACS Nano* **2010**, *4*, 6725−6734.
(17) Gómez-Graña, S.; Goris, B.; Altantzis, T.; Fernández-López, C.; Carbó-Argibay, E.; Guerrero-Martínez, A.; Almora-Barrios, N.; López, N.; Pastoriza-Santos, I.; Pérez-Juste, J.; Bals, S.; Van Tendeloo, G.; Liz-Marzán, L. M. *J. Phys. Chem. Lett.* **2013**, *4*, 2209−2216.
(18) Cho, E. C.; Camargo, P. H. C.; Xia, Y. *Adv. Mater.* **2010**, *22*, 744−748.
(19) Okuno, Y.; Nishioka, K.; Kiya, A.; Nakashima, N.; Ishibashi, A.; Niidome, Y. *Nanoscale* **2010**, *2*, 1489−1493.
(20) Yo, H.; Millstone, J. E.; Li, S.; Jang, J.-W.; Wei, W.; Wu, J.; Schatz, G. C.; Mirkin, C. A. *Nano Lett.* **2009**, *9*, 3038−3041.
(21) Langille, M. R.; Zhang, J.; Personick, M. L.; Li, S.; Mirkin, C. A. *Science* **2012**, *337*, 954−957.
(22) Xue, C.; Millstone, J. E.; Li, S.; Mirkin, C. A. *Angew. Chem., Int. Ed.* **2007**, *46*, 8436−8439.
(23) Langille, M. R.; Zhang, J.; Mirkin, C. A. *Angew. Chem., Int. Ed.* **2011**, *50*, 3543−3547.
(24) Yang, Y.; Wang, W.; Li, X.; Chen, W.; Fan, N.; Zou, C.; Chen, X.; Xu, X.; Zhang, L.; Huang, S. *Chem. Mater.* **2013**, *25*, 34−41.
(25) Li, C.; Sun, L.; Sun, Y.; Teranishi, T. *Chem. Mater.* **2013**, *25*, 2580−2590.
(26) Hong, S.; Choi, Y.; Park, S. *Chem. Mater.* **2011**, *23*, 5375−5378.
(27) Wu, H.-L.; Kuo, C.-H.; Huang, M. H. *Langmuir* **2010**, *26*, 12307−12313.
(28) Chiu, C.-Y.; Huang, M. H. *J. Mater. Chem. A* **2013**, *1*, 8081−8092.
(29) Huang, M. H.; Lin, P.-H. *Adv. Funct. Mater.* **2012**, *22*, 14−24.
(30) Liao, C.-W.; Lin, Y.-S.; Chanda, K.; Song, Y.-F.; Huang, M. H. *J. Am. Chem. Soc.* **2013**, *135*, 2684−2693.
(31) Chung, P.-J.; Lyu, L.-M.; Huang, M. H. *Chem.−Eur. J.* **2011**, *17*, 9746−9752.
(32) Wu, J.-K.; Lyu, L.-M.; Liao, C.-W.; Wang, Y.-N.; Huang, M. H. *Chem.−Eur. J.* **2012**, *18*, 14473−14478.
(33) Xia, X.; Zeng, J.; Oetjen, L. K.; Li, Q.; Xia, Y. *J. Am. Chem. Soc.* **2012**, *134*, 1793−1801.
(34) Langille, M. R.; Personick, M. L.; Zhang, J.; Mirkin, C. A. *J. Am. Chem. Soc.* **2012**, *134*, 14542−14554.
(35) Zhang, J.; Langille, M. R.; Mirkin, C. A. *J. Am. Chem. Soc.* **2010**, *132*, 12502−12510.
(36) Jiang, H.-L.; Akita, T.; Ishida, T.; Haruta, M.; Xu, Q. *J. Am. Chem. Soc.* **2011**, *133*, 1304−1306.
(37) Solanki, J. N.; Murthy, Z. V. P. *Ind. Eng. Chem. Res.* **2011**, *50*, 7338−7344.
(38) Chiu, C.-Y.; Chung, P.-J.; Lao, K.-U.; Liao, C.-W.; Huang, M. H. *J. Phys. Chem. C* **2012**, *116*, 23757−23763.